Journal of Inorganic Biochemistry 186 (2018) 10–16

Contents lists available at ScienceDirect

Journal of Inorganic Biochemistry

journal homepage: www.elsevier.com/locate/jinorgbio

Functional modeling of the MnCAT active site with a dimanganese(III) complex of an unsymmetrical polydentate N_3O_3 ligand

Gabriela N. Ledesma[a], Elodie Anxolabéhère-Mallart[b], Laurent Sabater[c], Christelle Hureau[c], Sandra R. Signorella[a,*]

[a] IQUIR (Instituto de Química Rosario), Consejo Nacional de Investigaciones Científicas y Técnicas (CONICET), Facultad de Ciencias Bioquímicas y Farmacéuticas, Universidad Nacional de Rosario, Suipacha 531, S2002LRK Rosario, Argentina
[b] Laboratoire d'Electrochimie Moléculaire UMR CNRS-P7 7591, Université Paris Diderot-Paris, 15 rue Jean-Antoine de Baïf, 75205 Paris Cedex 13, France
[c] CNRS, LCC (Laboratoire de Chimie de Coordination) and UPS, INPT, LCC, Université de Toulouse, 205 route de Narbonne, F-31077 Toulouse, France

ARTICLE INFO

Keywords:
Catalase activity
Dinuclear complexes
Manganese
Unsymmetrical N_3O_3-ligand

ABSTRACT

A new diMn^{III} complex, $[Mn_2L(OAc)_2(H_2O)](BPh_4)\cdot 3H_2O$ (**1**), obtained with the unsymmetrical N_3O_3-ligand H_3L = 1-[*N*-(2-pyridylmethyl),*N*-(2-hydroxybenzyl)amino]-3-[*N′*-(2-hydroxybenzyl),*N′*-(benzyl)amino]propan-2-ol, has been prepared and characterized. The unsymmetrical hexadentate ligand L^{3-} leads to coordination dissymmetry (dissimilar donor atoms) around each Mn ion (N_2O_4 and NO_4(solvent), respectively) leaving one labile site on one of the two Mn ions that facilitates interaction of the metal center with H_2O_2, as in Mn catalase. **1** is able to catalyze H_2O_2 disproportionation in acetonitrile, with second-order rate constant k_{cat} = 23.9(2) $M^{-1}\,s^{-1}$. The accessibility of the Mn_2^{II} state and the closeness of the two one-electron reduction processes suggest **1** employs Mn_2^{III}/Mn_2^{II} oxidation states for catalysis.

1. Introduction

Manganese catalase (MnCAT) catalyzes the disproportionation of H_2O_2 into innocuous H_2O and O_2 employing a diMn structural core $[Mn_2(\mu\text{-}O_2CR)(\mu\text{-}O/OH/H_2O)]$ (O_2CR = Glu) [1,2] that alternates between Mn_2^{II} and Mn_2^{III} oxidation states during catalysis [3–5]. Crystal structures of MnCAT enzymes isolated from *L. plantarum* [1] and *T. thermophilus* [2] revealed that the two metal ions of the diMn active site differ in the number of exchangeable water ligands, with only one of the Mn subsites bound to a labile water molecule that is proposed to be the initial substrate binding site during catalysis. This coordination dissymmetry around the two metal ions should be considered when designing mimics of these enzymes. However, most diMn complexes reported as MnCAT mimics have been prepared with symmetric dinucleating ligands that afford synthetic models with identical environment around the two metal centers [6–8]. Only unsymmetrical phenoxo-bridged diMn complexes have been evaluated as CAT-mimics, but in these compounds the phenoxo bridge leads to long intermetallic separation and, consequently, these complexes are less relevant as MnCAT models [9–12]. Therefore, there is a need to obtain analogues of these enzymes employing unsymmetrical ligands to reproduce the singularities of the biosite. The dinucleating ligand H_3L (H_3L = 1-[*N*-(2-pyridylmethyl),*N*-(2-hydroxybenzyl)amino]-3-[*N′*-(2-hydroxybenzyl),*N′*-(benzyl)amino]propan-2-ol) is an unsymmetrical diamine that provides two different coordination compartments and can be used to mimic bimetallic sites with different environment around the two metal centers [13]. This and other ligands of the same family have already been used to generate mononuclear Mn^{III}L [14] and trinuclear $[Mn_3^{III}(\mu\text{-}OH)(OAc)L_2]^+$ complexes [15]. We have decided to explore the possibility of obtaining dinuclear manganese complexes employing the same ligand, in order to assess the influence of the ligand asymmetry on the CAT activity of diMn mimics. With this aim, we report here the synthesis, characterizations, redox properties and CAT activity of a diMn^{III} complex obtained with the N_3O_3-hexadentate ligand H_3L and compare its reactivity with that of other dinuclear manganese catalysts.

2. Experimental part

2.1. Materials

All reagents were used as received, without further purification. Ligand H_3L was prepared according to a previously reported method [13]. Solvents were purified by standard procedures [16].

* Corresponding author.
E-mail address: signorella@iquir-conicet.gov.ar (S.R. Signorella).

https://doi.org/10.1016/j.jinorgbio.2018.04.023
Received 30 December 2017; Received in revised form 9 April 2018; Accepted 29 April 2018
Available online 18 May 2018

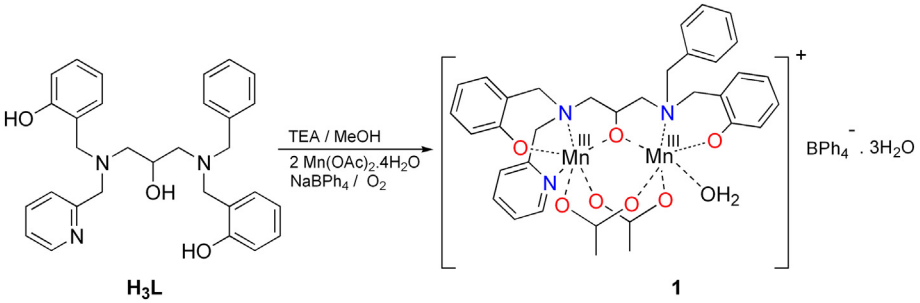

Scheme 1. Synthesis of complex **1**.

2.2. Analytical and physical measurements

Infrared spectra were recorded on a Perkin-Elmer Spectrum One FT-IR spectrophotometer in the 4000–400 cm^{-1} range. UV–visible spectra were recorded on a Jasco V-550 spectrophotometer, with thermostated cell compartments. Metal content was determinated by atomic absorption measurements on a Metrolab 250 AA spectrophotometer. Electrospray ionization (ESI) mass spectra were obtained with a Thermo Scientific LCQ Fleet. The solutions for electrospray were prepared from solutions of complex or reaction mixtures in acetonitrile, with a $\sim 10^{-5}$ M concentration. Cyclic voltammetry was recorded with an Autolab PG STAT 20 potentiostat. The counter electrode was a Pt wire, the reference electrode was a calomel electrode isolated in a fritted bridge, and the working electrode was a glassy carbon disk (diameter = 3 mm). Studies were carried out under Ar, in dry acetonitrile (ACROS) using 0.1 M tetrabutylammonium hexafluorophosphate (NBu_4PF_6) as supporting electrolyte. Temperature was regulated with a Julabo circulation bath. The working electrode was carefully polished before each voltammogram with a 1 μm diamond paste, sonicated in an ethanol bath, washed with ethanol, and dried with compressed air. ^{1}H NMR spectra were recorded on a Bruker AC 300 NMR spectrometer at ambient probe temperature (ca. 25 °C). Chemical shifts (in ppm) are referenced to tetramethylsilane and paramagnetic NMR spectra were acquired employing superWEFT sequence, with acquisition time of 50 ms. Electron paramagnetic resonance (EPR) spectra were obtained on a Bruker ESP 300 E spectrometer with a microwave frequency generated with a Bruker ER 04 (9–10 GHz).

2.3. Synthesis of complex $[Mn_2L(OAc)_2(H_2O)](BPh_4)\cdot 3H_2O$ (1)

Triethylamine (0.15 mL; 1 mmol) was added to a solution of H_3L (0.1695 g; 0.35 mmol) in methanol (5 mL) and the mixture was stirred by 15 min. Separately, $Mn(OAc)_2.4H_2O$ (0.1740 g; 0.71 mmol) was dissolved in methanol (3 mL) and added slowly to the solution containing the deprotonated form of the ligand. The color of the homogeneous solution immediately changed from pale yellow to brown and the stirring was kept for 30 min. A solution of $NaBPh_4$ (0.1225 g; 0.36 mmol) in methanol (1.5 mL) was added to the mixture and stirred for additional 12 h. The formed brown powder was separated by filtration, washed with water and cold diethyl ether (3 × 2 mL) and dried under vacuum with P_2O_5. Yield: 99.3 mg (0.09 mmol, 25%). Anal. calcd. for $BC_{58}H_{58}Mn_2N_3O_8\cdot 3H_2O$: C 63.34%; H 5.87%; Mn 9.99%; N, 3.82%. Found: C 63.48%; H 5.99%; Mn 10.2%; N 3.73%. ESI-mass spectrometry (ESI-MS) (acetonitrile): m/z = 708.25 $[Mn_2L(OAc)_2]^+$, 649.33 $[Mn_2L(OAc)]^+$. Significant IR bands (KBr, ν cm^{-1}): 3430, 3133, 3054, 1580, 1480, 1425, 1268, 1150, 1114, 1032, 1017, 742, 706, 650, 614, 605. UV–vis λ_{max} nm (ε, $M^{-1}\,cm^{-1}$) in CH_3CN: 270 (3323); 310 (2902); 363 (sh); 504 (945). Retention factor (R_f) for **1** = 0.75 (stationary phase = cellulose; mobile phase = 1:1 acetonitrile:methanol). R_f for the free ligand (same conditions) = 0.98.

2.4. Evaluation of CAT activity

The CAT activity of **1** was tested by volumetric determination of the evolved O_2 after addition of H_2O_2 to a solution of the complex in acetonitrile. A vial flask containing a degassed solution of **1** and capped with a rubber septum was thermostated at 20 °C and connected through a cannula to a gas-measuring buret (precision of 0.1 mL). A solution of H_2O_2 previously thermostated (with $[H_2O_2]$:[complex] ratio in the range 125–1300:1; [complex] = 0.07–0.76 mM) was injected through the septum to the stirred complex solution, and the resulting volume of oxygen was measured with the buret.

3. Results and discussion

3.1. Synthesis and spectroscopic characterization

The hexadentate ligand H_3L was deprotonated with 3 equiv. of triethylamine (TEA) and then reacted with 2 equiv. of $Mn(OAc)_2\cdot 4H_2O$. Metal complexation was evidenced by the change in the color of the solution, from pale yellow to dark brown. It had been previously observed that acetate from the Mn^{II} salt deprotonates phenol groups of the ligand and facilitates coordination to the metal center [17–19]. In the case of H_3L, reaction mixtures carried out in absence of TEA did not reflect immediate color changes, evidencing the addition of extra base was required for rapid complex formation. The dinuclear manganese complex **1** (see Scheme 1) was precipitated upon addition of sodium tetraphenylborate, as a brown solid. Thin layer chromatography (TLC) of **1** using different mobile phases (in different ratios) and three different stationary phases (silica, alumina and cellulose) showed only one spot.

Fig. 1 shows IR spectra of the dimanganese complex **1**, together with trinuclear [15] and mononuclear [14] complexes obtained with the same ligand under different conditions, as well as free ligand H_3L [13]. The spectrum of **1** retains the fingerprint of the coordinated ligand but differs from those belonging to the mono- and trinuclear complexes, particularly in the regions corresponding to the stretching frequencies of the coordinated acetate ligands and BPh_4^- counteranion. Three bands at 614, 706 and 732 cm^{-1} together with a strong and sharp stretching band at $\sim$3055 cm^{-1} (Fig. S1) can be assigned to non-coordinated BPh_4^- counter anion while the intense bands centered at 1580 and 1430 cm^{-1} are assignable to the antisymmetrical and symmetrical stretching modes of bridging acetate of **1** [20,21] (absent in the mononuclear complex and different from the trinuclear complex where acetate is bound as a terminal ligand to one of the Mn ions). A broad band centered at 3430 cm^{-1} corresponding to non-coordinated water molecules also appears in the spectrum (Fig. S1).

The positive mode ESI-mass spectrum of a freshly prepared solution of **1** in acetonitrile shows peaks at m/z 731, 708 and 649 (inset in Fig. 2(a)), attributed to the monocationic species $[Mn_2L(OAc)_2Na]^+$, $[Mn_2L(OAc)_2]^+$ and $[Mn_2L(OAc)]^+$, respectively, thus confirming its chemical composition and retention of dinuclearity in solution. Mixed valence $[Mn_2L(OAc)_2Na]^+$ and $[Mn_2L(OAc)]^+$ species that appear in

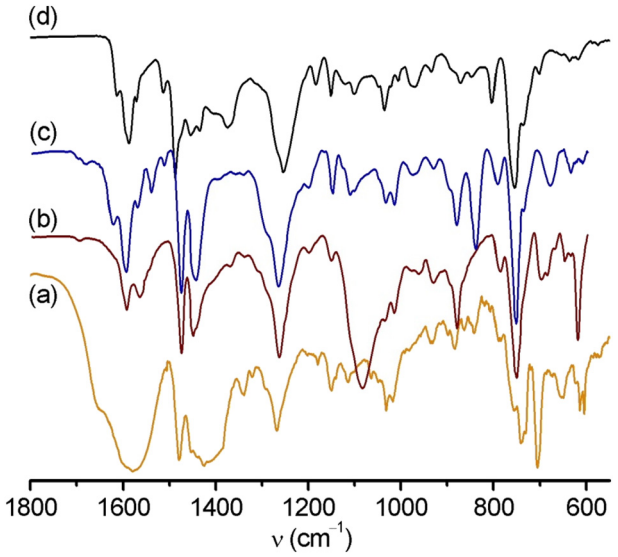

Fig. 1. FT-IR spectra of (a) **1**, (b) $[Mn_3L_2(OH)(OAc)]ClO_4$, (c) [MnL] and (d) H_3L.

the ESI-mass spectra of the complex are not observed by EPR spectroscopy, suggesting they are formed during the electrospray experiment. Tandem ESI-MS/MS of the species at *m/z* 708 showed that the peak at *m/z* 649 corresponds to the main fragment generated from the precursor ion (Fig. S2), thus supporting this mixed valence species is generated within the spectrometer. In the negative mode, the mass spectrum of **1** shows one peak at *m/z* 319, that confirms the presence of tetraphenylborate anion (Fig. S3).

The electronic spectrum of complex **1** shows absorptions at 250–300 nm associated to intraligand π-π* transitions, a shoulder in the range of 350–420 nm attributed to ligand-to-metal charge transfer transition (LMCT) from phenoxo/pyridyl to Mn^{III}, and a broad band centered at 504 nm that can be assigned to a *d-d* transition of the Mn^{III} ion overlapped with a LMCT band (Fig. 2(a)). The absorption coefficient $\varepsilon^{504} = 945\ M^{-1}\ cm^{-1}$ is in agreement with values previously informed for other related phenoxo diMn^{III} complexes [17,22–25]. Electronic spectra of **1** remained unchanged at least within 2 h after preparation of the solutions as do the ESI-mass spectra registered within this time interval. However, when the solution was left to stay for one or more days, spectral changes were observed and new peaks appeared in the ESI-mass spectra besides those of the starting complex (Fig. S4). The appearance of peaks at *m/z* 1141 and 536 corresponding to the $[Mn_3L_2O]^+$ and $[MnLH]^+$ monocations in the mass spectra, indicates that the starting dinuclear complex can convert into mono- and trinuclear ones and an equilibrium can be attained with time, although in acetonitrile this process is slow. ESI-MS/MS of the species at *m/z* 1141 (Fig. S5) yields fragments at *m/z* higher than 760, so that $[MnLH]^+$ (*m/z* 536) is not generated from this peak, but exists in the solution. In Fig. 2(b), the electronic spectrum of a freshly prepared solution of **1** is compared to the spectra of equimolar solutions of mononuclear MnL and trinuclear $[Mn_3L_2(OH)(OAc)]^+$ complexes in acetonitrile. While the band at 504 nm is absent or is of very low intensity in the spectrum of the mononuclear complex, the trinuclear complex exhibits an intense band ($\varepsilon^{504} = 1500\ M^{-1}\ cm^{-1}$) at this wavelength. The trinuclear complex contains a dinuclear moiety with the two Mn ions bound to a ligand donor set similar to complex **1**, and the third Mn ion placed at the corner of an isosceles triangle, at a longer distance from the other two Mn ions [15]. So this band can be considered a common pattern for the dinuclear fragment of the Mn_2 and Mn_3 complexes formed with L^{3-}.

The ^1H NMR spectrum of a freshly prepared solution of **1** in CD_3OD (Fig. 3(a)) shows resonances outside the diamagnetic region spanning from 60 to −30 ppm. The spectral pattern comprises a set of broad signals (linewidth ≈ 750–1200 Hz) between 60 and 20 ppm, and two upfield relatively sharp signals (linewidth ≈ 200 Hz) at −20 and −28 ppm.

With the aim of identifying the bridging acetate resonance, Na(D_3CCO_2) was added to the solution of **1** in CD_3OD. Fig. 3(b–f) displays the spectra registered after addition of 0.1 to 2.0 equiv. of D_3-acetate to the solution of **1**. The full spectral pattern did not change upon addition of acetate, indicating the retention of the coordination mode of the ligand. However, a decrease of the resonance at 30 ppm can be observed with increasing amount of deuterated acetate (Fig. 3(a–f)). A signal at around 30 ppm has been reported for several Mn^{III}_2(μ-OAc) complexes [26–28], and has been attributed to the methyl group of the bridging acetate. Consequently, the decrease of this signal can result from exchange of bridging acetate by deuterated acetate with no effect on any other resonance. Additionally, this resonance is not present in the ^1H NMR spectra of mononuclear MnL (lacking acetate) or trinuclear $[Mn_3L_2(\mu\text{-}OH)(OAc)]^+$ (which has terminally bound acetate) complexes (Fig. S6), thus reinforcing the assignment of this signal to bridging acetate.

It has been shown that diMn^{III} complexes with terminal acetate show a broad signal at around 1.9 ppm which differentiates from the

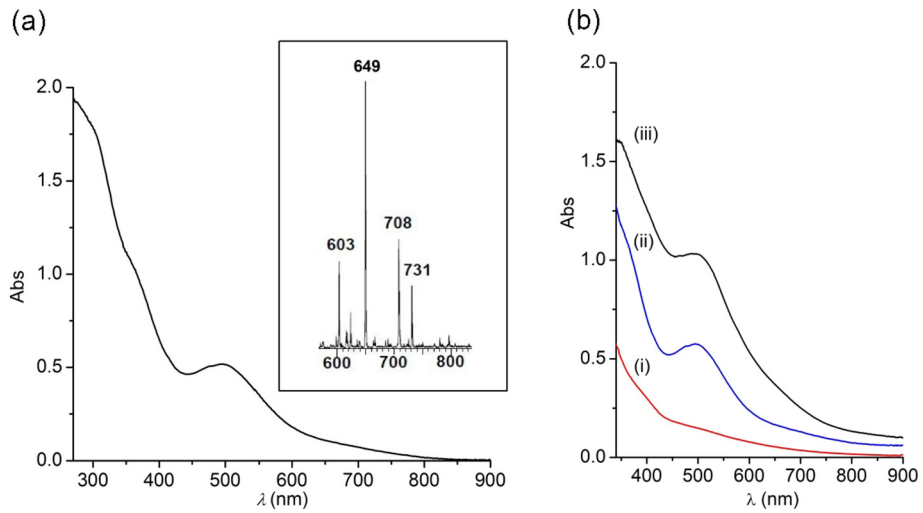

Fig. 2. (a) Electronic spectrum of 0.59 mM **1** in acetonitrile. T = 20 °C, l = 1 cm. Inset: ESI-mass spectrum of **1** in acetonitrile. (b) Comparative spectra of equimolar solutions of MnL (i), **1** (ii) and $[Mn_3L_2(OH)(OAc)]^+$ (iii) in acetonitrile. [complex] = 0.67 mM.

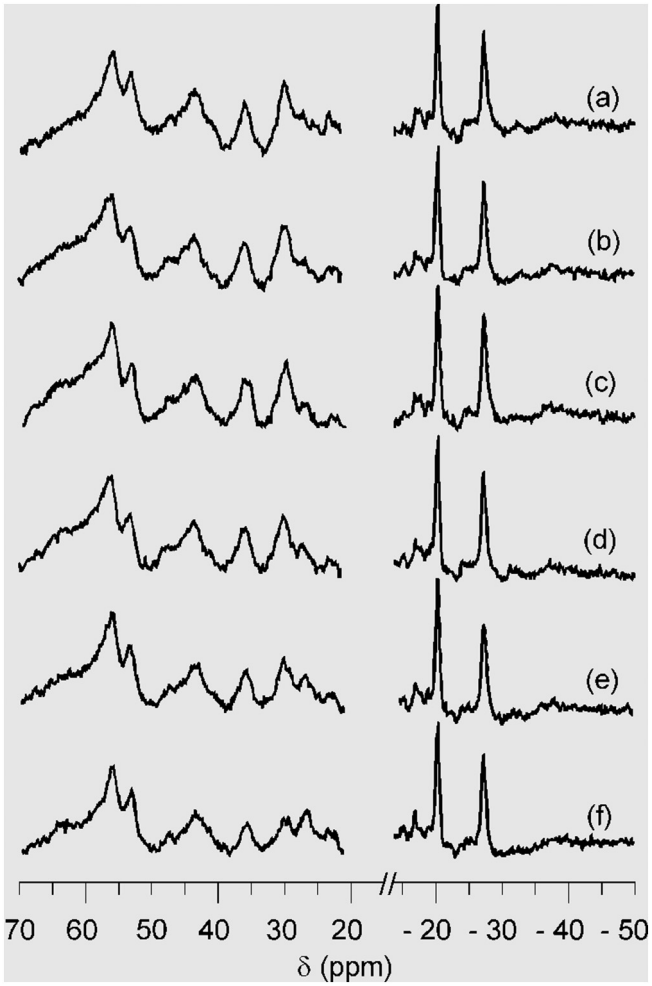

Fig. 3. ^{1}H NMR spectra of complex **1** (4 mM) before (a) and after the addition of (b) 0.1, (c) 0.2, (d) 0.5, (e) 1 and (f) 2 equiv. of $Na(D_3CCO_2)$ in CD_3OD, at 25 °C. Equilibration time: 25 min after each addition of $Na(D_3CCO_2)$.

sharp signal of free acetate at 1.89 ppm [29]. In the present case, no signal attributable to terminally coordinated acetate was observed in the diamagnetic region of the spectrum of complex **1**. These results suggest that the most plausible structure for complex **1** in solution contains two bridging acetate ligands (as shown in Scheme 1) and corresponds to only one stereoisomer (not a mixture) as pointed by the unique spot observed by TLC using multiple mobile and stationary phases. The lack of crystal structure (several attempts to crystallize **1** failed) disables to know which of the stereoisomers has formed (Scheme S1 shows possible stereoisomers for **1** that are consistent with spectroscopic results).

3.2. Electrochemical studies

The electrochemical behavior of complex **1** was studied by cyclic voltammetry in acetonitrile solutions, using a glassy carbon electrode (Figs. 4(a) and S7). At 20 °C, the cyclic voltammogram of **1** shows one irreversible anodic wave at $E^{pa1} \approx 0.4$ V vs saturated calomel electrode (SCE) attributed to the oxidation of Mn_2^{III} to $Mn_2^{III,IV}$, with an irreversible reduction at $E^{pc1} \approx 0.2$ V vs SCE, and two cathodic waves at $E^{pc2} \approx -0.25$ V and $E^{pc3} = -0.52$ V vs SCE, that can be assigned to two successive one-electron reduction processes $Mn_2^{III}/Mn_2^{II,III}$ and $Mn_2^{II,III}/Mn_2^{II}$, respectively. An additional intense anodic wave can be observed $E \approx 0.9$ V vs SCE, corresponding to the oxidation of the BPh_4^- counteranion (Fig. S7). These processes were absent in voltammograms of the free ligand, which exhibit oxidation waves at potentials higher than 0.9 V belonging to the oxidation of phenol, alcohol and pyridine groups [14].

Bulk electrolysis of **1** at −0.55 V (vs SCE) in acetonitrile results in the decrease of the intensity of the band at 500 nm and the shoulder at 380 nm (Fig. 4(b)), confirming the cathodic waves correspond to the reduction of the Mn_2^{III} to Mn_2^{II} center.

Electrochemical behavior of **1** is well different from the mononuclear MnL that only shows a one-electron irreversible anodic process at $E^{pa} = 0.53$ V vs SCE attributed to the Mn^{III} to Mn^{IV} oxidation [14]. Also, the trinuclear $[Mn_3L_2(\mu\text{-OH})(OAc)]^+$ complex displays a different cyclic voltammogram compared to **1**, with two cathodic peaks at $E^{pc1} = -0.175$ and $E^{pc2} = -0.7$ V vs SCE attributed to two one-electron reductions of the $Mn^{III}(\mu\text{-phenoxo})(\mu\text{-alkoxo})Mn^{III}$ fragment, and one anodic peak at $E^{pa1} = 0.505$ V vs SCE, assigned to the one-electron oxidation of the apical Mn^{III} ion bound to terminal acetate [15]. Therefore, **1** can be oxidized at a potential lower than both mononuclear MnL and trinuclear $[Mn_3L_2(\mu\text{-OH})(OAc)]^+$ complexes and can be reduced through a two-electron process at a potential slightly less negative than $[Mn_3L_2(\mu\text{-OH})(OAc)]^+$.

3.3. Catalytic activity studies

The ability of **1** for catalyzing the disproportionation of H_2O_2 into O_2 and H_2O was evaluated in acetonitrile. Addition of H_2O_2 to a recently prepared solution of **1** produces immediate evolution of molecular oxygen, together with a slight change in the color of the solution. The O_2 evolution was evaluated in excess of H_2O_2 and at constant temperature by volumetric measurement of evolved O_2, and the dependence of the reaction rate with [catalyst] and $[H_2O_2]_0$ was determined by varying [catalyst] at fixed $[H_2O_2]_0$ (Fig. 5), and varying the $[H_2O_2]_0$ at constant [catalyst] (Fig. 6). At constant $[H_2O_2]_0 = 100$ mM, the reaction exhibits first-order kinetics on [catalyst] (Fig. 5 (right)), with first-order rate constant $k = 3.46(9)\ s^{-1}$. At fixed [catalyst] = 0.3 mM, initial rates show a good linear dependence on $[H_2O_2]_0$ indicating the reaction is first-order on $[H_2O_2]$. The second-order catalytic constant $k_{cat} = 23.9(2)\ M^{-1}\ s^{-1}$ was obtained from the slope of the plot of r_i/[catalyst] vs $[H_2O_2]_0$ (Fig. 6 (right)).

Complex **1** can convert more than 300 equiv. of H_2O_2 into O_2 and H_2O. However, the initial rate of H_2O_2 dismutation gradually decreases with successive additions of excess H_2O_2 to the solution of catalyst. Fig. 7(a,b) shows the O_2 generated from two successive additions of 100 equiv. H_2O_2 over an acetonitrile solution of **1** for which the measured initial rate decreased 15% from the first to the second addition. Room-temperature UV–vis absorption spectra were taken during the progress of the reaction of **1** with excess of H_2O_2. After addition of 100 equiv. of H_2O_2 to a solution of **1** in acetonitrile the band at 504 nm remained essentially unchanged until the end of the reaction (Fig. 7(c)). After a second addition of 100 equiv. of H_2O_2, the intensity of the band at 504 nm (Fig. 7(c)) decreased down to 85% of the initial value while the shoulder at ca. 370 nm grew 15% up. ESI-mass spectra taken during and at the end of the reaction of a 100:1 H_2O_2:**1** mixture showed the same peaks as the starting solution (Fig. 7(d)), meaning that the initial complex still remains in solution under these conditions. Notably, the reaction mixtures are EPR silent. No Mn_2^{II} nor $Mn^{II}Mn^{III}$ ($Mn^{III}Mn^{IV}$) mixed-valence species characterized by multiline spectrum centered at $g = 2$, were observed, during or at the end of the reaction. Besides, uncoupled Mn^{II} was not observed at any time in the reaction mixture.

When more than 200 equiv. of H_2O_2 were added over **1**, the band at 504 nm diminished progressively and disappeared while the solution became turbid, probably as the result of the formation of a poorly soluble inactive form of the complex. Concurrently the rate of O_2 evolution also became slower when larger excess of H_2O_2 was added over **1** (Fig. S8), although the stoichiometric amount of O_2 was still released.

In complex **1**, the hexadentate ligand leads to coordination dissymmetry (dissimilar donor atoms) around each Mn ion (N_2O_4 and NO_4(solvent), respectively) leaving one labile site on one of the two Mn

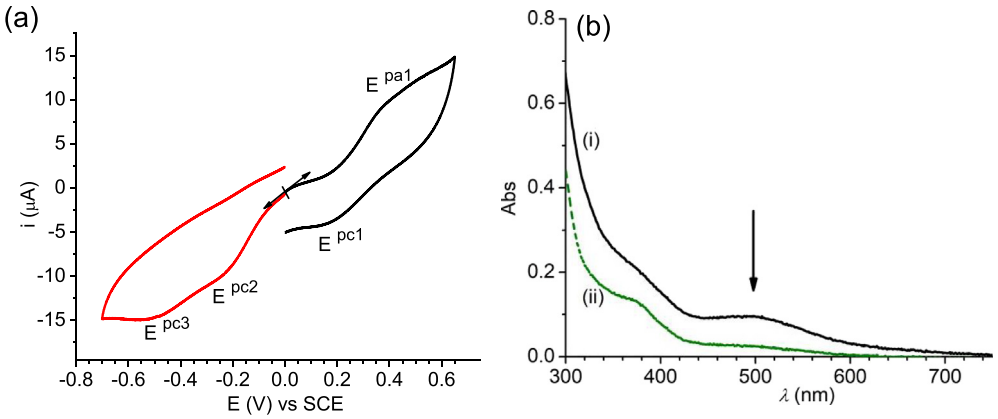

Fig. 4. (a) Cyclic voltammogram of 1.15 mM **1** in acetonitrile, 0.1 M $TBAPF_6$ under argon; scan rate: 100 mV/s; T = 20 °C. (b) UV–vis absorption spectra of **1** recorded before (i) and after electrolysis at −0.55 V (ii); conditions: 0.88 mM in acetonitrile, 0.2 M $TBAPF_6$, T = 0 °C, optical path 2 mm.

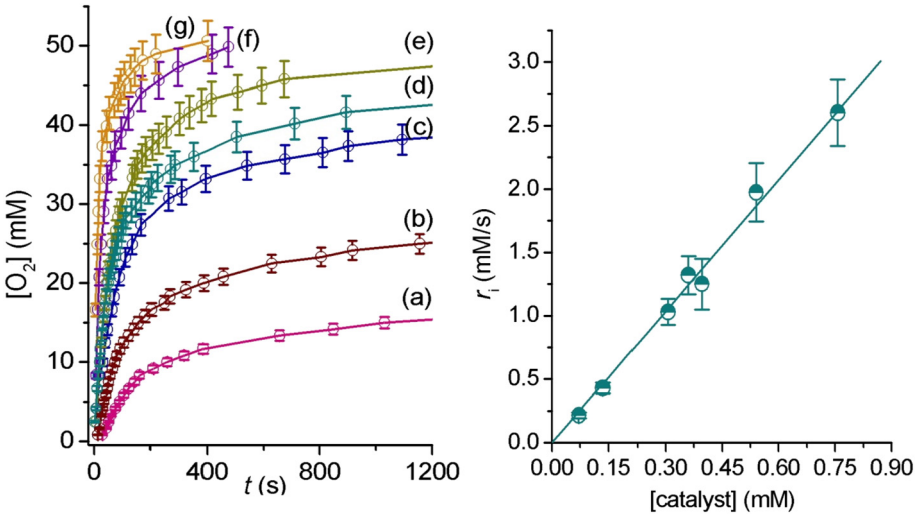

Fig. 5. Left: time-evolution of $[O_2]$ from mixtures of H_2O_2 (100 mM) and (a) 0.073, (b) 0.13, (c) 0.20, (d) 0.31, (e) 0.40, (f) 0.55 and (g) 0.76 mM of **1**, in 5.0 mL MeCN, T = 20 °C. Right: Linear dependence of initial rates on the catalyst concentration.

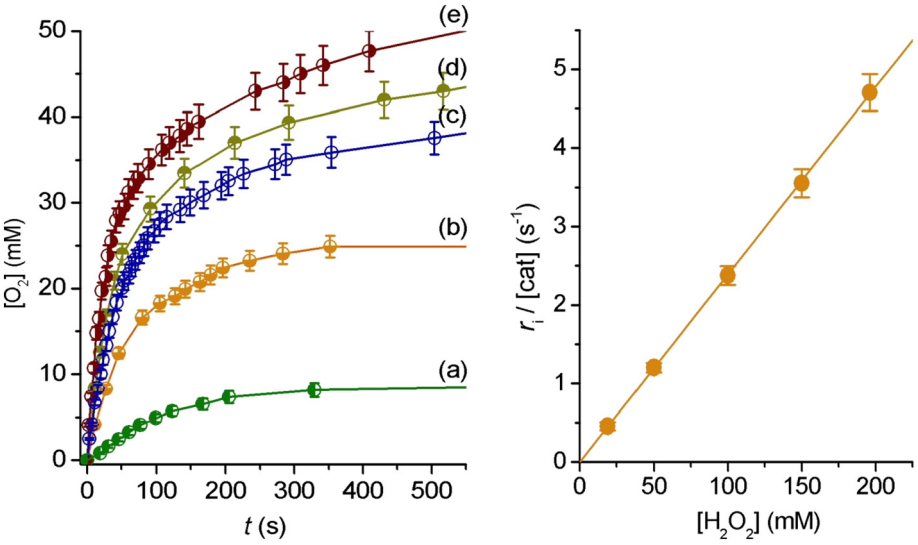

Fig. 6. Left: Time-evolution of $[O_2]$ from mixtures of 0.30 mM **1** and (a) 19, (b) 50, (c) 100, (d) 150 and (e) 196 mM H_2O_2 in 5.0 mL of MeCN. T = 20 °C. Right: Linear dependence of initial rates vs $[H_2O_2]$.

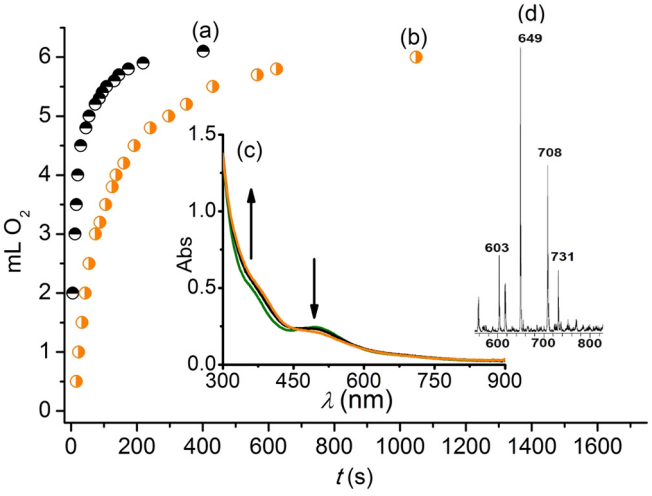

Fig. 7. O_2 evolution after (a) first and (b) second addition of 130 equiv. of H_2O_2 over 0.76 mM **1**, in MeCN at 20 °C. (c) UV–vis spectra of **1** (0.25 mM) before (green line) and after first (black line) and second addition (orange line) of 100 equiv. of H_2O_2, in MeCN. (d) Mass spectrum of complex **1** at the end of the reaction with 100 equiv. H_2O_2, in MeCN. (For interpretation of the references to color in this figure legend, the reader is referred to the web version of this article.)

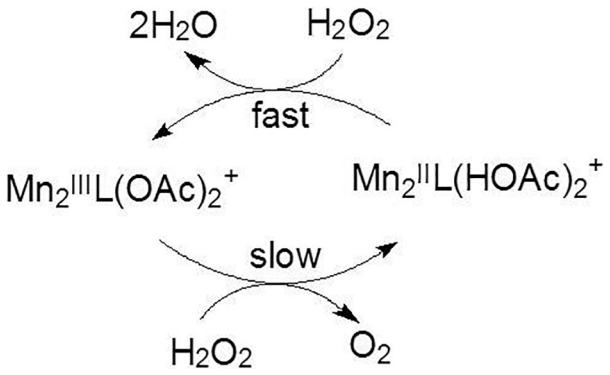

Scheme 2. Proposed catalytic cycle for disproportionation of H_2O_2 by **1**.

ions that should facilitate interaction of the metal center with H_2O_2. This labile site on one of the Mn ions might favor terminal H_2O_2 binding, while acetate bridges could serve as proton storage sites. Therefore, the catalytic cycle can initiate upon binding of peroxide to the Mn ion with the exchangeable solvent molecule, while deprotonation of H_2O_2 can be assisted by the bridging carboxylate groups. No EPR signal is observed during the H_2O_2 disproportionation reaction, in line with Mn_2^{III} (EPR silent) being the major form of the catalyst during the reaction. This is in agreement with electronic spectroscopy and mass spectrometry results. Given the complex can be reduced by two electrons and the two reduction processes are close (see electrochemical results above) it seems reasonable to propose that **1** employs Mn_2^{III}/Mn_2^{II} oxidation states for catalysis, with reduction of catalyst occurring in the limiting slow step (Scheme 2).

3.4. Comparison to other complexes

The initial rate (r_i) of H_2O_2 disproportionation catalyzed by the dinuclear complex **1** is in the same range as other diMn complexes of alkoxo-bridging ligands (Table 1, entries 2–3), although slower than for complexes with bis(alkoxo) diMn cores (Table 1, entries 4–5). Either alkoxo- or bis(alkoxo)-bridged diMn complexes show better CAT activity than phenoxo-bridged diMn complexes (Table 1, entries 6–8) with long Mn···Mn distances (≈3.5 Å) and where the central phenolate sits askew the metal-metal axis [9,32]. In **1**, the low reduction potential could be compensated by the presence of the labile coordination site on the diMn center to react with the substrate through an inner-sphere mechanism, resulting in an intermediate activity for H_2O_2 disproportionation. Even when solvent, temperature and oxidation states involved during catalysis are different for the various complexes listed in Table 1, the bis-alkoxo bridging motif appears as the best for catalytic disproportionation of H_2O_2 by diMn complexes, probably because the additional methoxo bridge shortens the Mn···Mn separation (2.91–2.95 Å in bis(alkoxo)-bridged [17,31] vs ≈3.2 Å in alkoxo-bridged $diMn^{III}$ complexes [30]) facilitating communication between the two Mn centers, and is an internal base better than carboxylate to assist proton transfer during the redox reaction.

4. Conclusions

Reaction of the hexadentate N_3O_3-ligand L^{3-} with 2 equiv. of $Mn(OAc)_2$ and 1 equiv. of $NaBPh_4$ in basic medium affords the dinuclear

Table 1
Kinetics parameters for complex **1** and other selected CAT mimics.

	Catalyst	r_i[a] (mM H_2O_2 mM cat^{-1} min^{-1})	Solvent, T (°C)	Bridging groups	Oxidation states[b]	E[c] (V) vs SCE	Ref.
1	**1**	14.3	MeCN, 20	Alkoxo-bis(carboxylate)	Mn_2^{III}/Mn_2^{II}	−0.25[d]	This work
2	$[Mn_2(\mu\text{-OAc})_2(5\text{-Cl-hppnO})]^+$	22.6	DMF, 25	Alkoxo-bis(carboxylate)	Mn_2^{III}/Mn_2^{II}	−0.2[d]	[30]
3	$[Mn_2(\mu\text{-OH}_2)(OAc)(benzimpnO)]^{2+}$	19.5	MeOH:H_2O, 25	Alkoxo-aquo	Mn_2^{III}/Mn_2^{II}	0.79[e]	[29]
4	$[Mn_2(\mu\text{-OMe})(\mu\text{-OAc})(hppentO)]^+$	58.5	DMF, 10	Bis(alkoxo)carboxylate	Mn_2^{III}/Mn_2^{II}	−0.04	[17]
5	$[Mn_2(\mu\text{-OMe})(\mu\text{-OAc})(salpentO)]^+$	46.1	DMF, 25	Bis(alkoxo)carboxylate	Mn_2^{III}/Mn_2^{IV}	0.38	[31]
6	$[Mn_2(bpbpmp)(OAc)_2]^{2+}$	8.7	MeCN, 0	Phenoxo-bis(carboxylate)	$Mn_2^{II,III}/Mn_2^{III,IV}$	1.28[d]	[11]
7	$[Mn_2(bpbp)(\mu\text{-OAc})_2]^{2+}$	2.23	MeOH, 0	Phenoxo-bis(carboxylate)	$Mn_2^{II,III}/Mn_2^{III,IV}$	1.09	[9,32]
8	$[Mn_2(bprol\text{-}^tBu\text{-}p)(\mu\text{-OAc})(H_2O)_2]^{2+}$	0.17	DMF, 20	Phenoxo-carboxylate	Mn_2^{III}/Mn_2^{II}	NR	[33]

benzimidazolylpnOH = *N,N,N′,N′*-tetrakis(2-methylenebenzimidazolyl)-1,3-diaminopropan-2-ol. bpbp = 2,6-bis{[bis(2-pyridylmethyl)amino]methyl}-4-tert-butylphenolato. bpbpmp = 2-[bis(2-pyridylmethyl)aminomethyl]-6-{[(benzyl)(2-pyridylmethyl)amino]methyl}-4-methylphenol. bphpmp = 2-[bis(2-pyridylmethyl)aminomethyl]-6-{[(2-hydroxybenzyl)(2-pyridylmethyl)amino]methyl}-4-methylphenol. H_3bprol-^{t}Bu-p = 2,6-bis(prolin-1-yl)methyl-4-t-butylphenol. hppentOH = 1,5-bis[(2-hydroxy-5-X-benzyl)(2-pyridylmethyl)amino]pentan-3-ol. hppnOH = 1,3-bis[(2-hydroxybenzyl)(2-pyridylmethyl)amino]propan-2-ol. salpentOH = 1,5-bis(salicylidenamino)pentan-3-ol.
Schemes of the complexes are given in the SI.

[a] r_i values were calculated from reported kinetic data. [catalyst] = 10 μM; [H_2O_2] = 10 mM.
[b] Oxidation states during catalysis.
[c] Potentials for one-electron redox processes.
[d] Irreversible.
[e] Bielectronic redox process. NR = not reported.

complex $[Mn_2L(OAc)_2(H_2O)]BPh_4 \cdot 3H_2O$ (**1**). The obtention of this complex evidences the versatility of L^{3-}, which gives mono- [14], di- or trinuclear [15] complexes depending on the reaction conditions. IR and NMR spectroscopic pattern of **1** shows unique features that distinguishes this complex from MnL and $[Mn_3L_2(\mu\text{-OH})(OAc)]ClO_4$. Electronic spectra of complexes **1** and trinuclear $[Mn_3L_2(\mu\text{-OH})(OAc)]^+$ share an absorption band around 500 nm, absent in MnL, associated to the alkoxo-bridged Mn^{III}_2 fragment. Electrochemical behavior of **1** also differentiates from the mono- and trinuclear counterparts and provides an additional way to identify the nuclearity of the complex in solution.

Complex **1** disproportionates H_2O_2 in acetonitrile with first-order kinetics on both [catalyst] and $[H_2O_2]$. Given the six coordination sites of one of the Mn ions are occupied by donor sites of the ligand and bridging carboxylate groups, initial binding to the substrate must occur at the Mn ion with a labile coordination site, with bridging acetates as internal bases to assist substrate deprotonation coupled to the redox reaction [29]. These two factors (labile coordination site and endogenous base) might compensate the low oxidizing power of **1**, enabling this compound to catalyze H_2O_2 disproportionation through an inner-sphere mechanism at a similar rate as other alkoxo-bridged diMn complexes.

Acknowledgements

We thank the National University of Rosario (BIO401), CONICET (PIP 0337) and CNRS (PICS 263815) for financial support.

Appendix A. Supplementary data

Supplementary data to this article can be found online at https://doi.org/10.1016/j.jinorgbio.2018.04.023.

References

[1] V.V. Barynin, M.M. Whittaker, S.V. Antonyuk, V.S. Lamzin, P.M. Harrison, P.J. Artymyuk, J.M. Whittaker, Structure 9 (2001) 725–738.
[2] S.V. Antonyuk, V.R. Melik-Adamyan, A.N. Popov, V.S. Lamzin, P.D. Hempstead, P.M. Harrison, P.J. Artymyuk, V.V. Barynin, Crystallogr. Rep. 45 (2000) 105–116.
[3] P.J. Riggs-Gelasco, R. Mei, J.E. Penner-Hahn, H.H. Thorp, V.L. Pecoraro (Eds.), Mechanistic Bioinorganic Chemistry, American Chemical Society, Washington, DC, 1995(Chapter 8).
[4] W.C. Stallings, K.A. Pattridge, R.A. Strong, M.L. Ludwig, J. Biol. Chem. 260 (1985) 16424–16432.
[5] S. Signorella, C. Palopoli, V. Daier, G. Ledesma, R.H. Kretsinger, E.A. Permyakov, V.N. Uversky (Eds.), Encyclopedia of Metalloproteins, Springer, New York, 2013, pp. 1283–1292.
[6] S. Signorella, C. Hureau, Coord. Chem. Rev. 256 (2012) 1229–1245.
[7] S. Abdolahzadeh, J.W. de Boer, W.R. Browne, Eur. J. Inorg. Chem. (2015) 3432–3456.
[8] A.J. Wu, J.E. Penner-Hahn, V.L. Pecoraro, Chem. Rev. 104 (2004) 903–938.
[9] R. Singh, M. Haukka, C.J. McKenzie, E. Nordlander, Eur. J. Inorg. Chem. (2015) 3485–3492.
[10] P. Karsten, A. Neves, A.J. Bertoluzzi, J. Strahle, C. Maichle-Mossmer, Inorg. Chem. Commun. 5 (2002) 434–438.
[11] L. Dubois, D.-F. Xiang, X.-S. Tan, J.-M. Latour, Eur. J. Inorg. Chem. (2005) 1565–1571.
[12] L. Dubois, R. Caspar, L. Jacquamet, P.-E. Petit, M.-F. Charlot, C. Baffert, M.-N. Collomb, A. Deronzier, J.-M. Latour, Inorg. Chem. 42 (2003) 4817–4827.
[13] G.N. Ledesma, S.R. Signorella, Tetrahedron Lett. 53 (2012) 5699–5702.
[14] G.N. Ledesma, H. Eury, E. Anxolabéhère-Mallart, C. Hureau, S.R. Signorella, J. Inorg. Biochem. 146 (2015) 69–76.
[15] G.N. Ledesma, E. Anxolabéhère-Mallart, E. Rivière, S. Mallet-Ladeira, C. Hureau, S.R. Signorella, Inorg. Chem. 53 (2014) 2545–2553.
[16] D.D. Perrin, W.L.F. Armarego, Purification of Laboratory Chemicals, third ed., Pergamon Press, Oxford, 1988.
[17] H. Biava, C. Palopoli, C. Duhayon, J.P. Tuchagues, S. Signorella, Inorg. Chem. 48 (2009) 3205–3214.
[18] C. Palopoli, G. Gómez, A. Foi, F. Doctorovich, S. Mallet-Ladeira, C. Hureau, S. Signorella, J. Inorg. Biochem. 167 (2017) 49–59.
[19] C. Palopoli, C. Duhayon, J.P. Tuchagues, S. Signorella, Dalton Trans. 43 (2014) 17145–17155.
[20] G.B. Deacon, R.J. Phillips, Coord. Chem. Rev. 33 (1980) 227–250.
[21] K. Nakamoto, Infrared and Raman Spectra of Inorganic and Coordination Compounds, 5th ed., Wiley-Interscience, New York, 1997, p. 60 (Part B).
[22] L. Dubois, D.F. Xiang, S.S. Tan, J. Pecaut, P. Jones, S. Baudron, L. Le Pape, J.M. Latour, C. Baffer, S. Chardon-Noblat, M.N. Collomb, A. Deronzier, Inorg. Chem. 42 (2003) 750–760.
[23] M. Hirotsu, M. Kojima, W. Mori, Y. Yoshikawa, Bull. Chem. Soc. Jpn. 71 (1998) 2873–2884.
[24] A. Neves, S.M.D. Erthal, I. Vencato, A.S. Ceccato, Y.P. Mascarehas, O.R. Nascimento, M. Hörner, A.A. Batista, Inorg. Chem. 31 (1992) 4749–4755.
[25] C. Hureau, L. Sabater, F. Gonnet, G. Blain, J. Sainton, E. Anxolabéhère-Mallart, Inorg. Chim. Acta 359 (2006) 339–345.
[26] M.R. Bermejo, A.M. González, M. Fondo, A. García-Deibe, M. Maneiro, J. Sanmartín, O. Hoyos, M. Watkinson, New J. Chem. 24 (2000) 235–241.
[27] M.T. Caudle, P. Riggs-Gelasco, A.K. Gelasco, J.E. Penner-Hahn, V.L. Pecoraro, Inorg. Chem. 35 (1996) 3577–3584.
[28] D.W. Wright, H.J. Mok, C.E. Dubé, W.H. Armstrong, Inorg. Chem. 37 (1998) 3714–3718.
[29] A.E.M. Boelrijk, G.C. Dismukes, Inorg. Chem. 39 (2000) 3020–3028.
[30] S. Signorella, J.-P. Tuchagues, D. Moreno, C. Palopoli, J.G. Hughes, A.J. Robinson (Eds.), Inorganic Biochemistry Research Progress, Nova Sci. Publ. Inc., New York, 2008.
[31] C. Palopoli, B. Chansou, J.P. Tuchagues, S. Signorella, Inorg. Chem. 39 (2000) 1458–1462.
[32] R.K. Seidler-Egdal, F.B. Johansson, S. Veltzé, E.M. Skou, A.D. Bond, C.J. McKenzie, Dalton Trans. 40 (2011) 3336–3345.
[33] J. Kaizer, R. Csonka, G. Speier, React. Kinet. Catal. Lett. 94 (2008) 157–163.